Neuron
Article

# Unique Properties of Mesoprefrontal Neurons within a Dual Mesocorticolimbic Dopamine System

Stephan Lammel,[1,3] Andrea Hetzel,[3,4] Olga Häckel,[3,4] Ian Jones,[3,5] Birgit Liss,[2,3,*] and Jochen Roeper[1,3,*]
[1]Institute of Neurophysiology, Neuroscience Center, Goethe-University Frankfurt, Frankfurt 60590, Germany
[2]Molecular Neurophysiology, Institute for General Physiology, University Ulm, Ulm 89081, Germany
[3]Department of Physiology, Marburg University, Marburg 35032, Germany
[4]These authors contributed equally to this work.
[5]Present address: JT International S.A., Geneva, Switzerland.
*Correspondence: birgit.liss@uni-ulm.de (B.L.), roeper@em.uni-frankfurt.de (J.R.)
DOI 10.1016/j.neuron.2008.01.022

## SUMMARY

**The mesocorticolimbic dopamine system is essential for cognitive and emotive brain functions and is thus an important target in major brain diseases like schizophrenia, drug addiction, and attention deficit hyperactivity disorder. However, the cellular basis for the diversity in behavioral functions and associated dopamine-release pattern within the mesocorticolimbic system has remained unclear. Here, we report the identification of a type of dopaminergic neuron within the mesocorticolimbic dopamine system with unconventional fast-firing properties and small DAT/TH mRNA expression ratios that selectively projects to prefrontal cortex and nucleus accumbens core and medial shell as well as to basolateral amygdala. In contrast, well-described conventional slow-firing dopamine midbrain neurons only project to the lateral shell of the nucleus accumbens and the dorsolateral striatum. Among this dual dopamine midbrain system defined in this study by converging anatomical, electrophysiological, and molecular properties, mesoprefrontal dopaminergic neurons are unique, as only they do not possess functional somatodendritic Girk2-coupled dopamine D2 autoreceptors.**

## INTRODUCTION

The dopamine midbrain system is not only involved in motor control and movement disorders like Parkinson disease, but also plays a crucial part in many emotional and cognitive functions of the brain and its major disturbances in schizophrenia, drug addiction, and attention deficit hyperactivity disorder (ADHD) (Bjorklund and Dunnett, 2007b). These latter functions are mediated to a large degree by the mesocorticolimbic dopamine system, which is comprised of dopaminergic (DA) midbrain projections from the ventral tegmental area (VTA, A10) and the neighboring substantia nigra (SN, A9) to cortical territories and subcortical limbic areas including, prominently, the shell and the core regions of the nucleus accumbens (NAc) and the basolateral amygdala (BLA) (Bjorklund and Dunnett, 2007a). Given this degree of physiological and pathophysiological diversity within the dopaminergic midbrain system, more selective pharmacological targeting of its distinct projections is a highly desired goal to prevent common side effects of conventional treatments occurring in, for example, schizophrenia Fleischhacker and Widschwendter, 2006) and Parkinson disease (Weintraub and Stern, 2005).

However, while the neuroanatomical connectivity of the mesocorticolimbic DA system has been extensively studied in rodents and primates (Bjorklund and Dunnett, 2007a; Haber, 2003), its functional and molecular properties are less well defined. Even at the level of the well-studied basic electrophysiological properties of DA midbrain neurons (Grace et al., 2007; Schultz, 2007), the degree of functional diversity associated with distinct axonal targets remains unresolved. Schultz and colleagues have successfully defined the computational roles of tonic and phasic discharge patterns of conventional DA midbrain neurons in reward-prediction error and uncertainty signaling (Fiorillo et al., 2003; Schultz, 2007; Tobler et al., 2005). However, the neurophysiological basis for the slower and more sustained pattern of DA release in, for example, cortical target areas during different behavioral contexts, more related to salience (Bassareo et al., 2002; Berridge, 2007; Di Chiara and Bassareo, 2007), effort (Salamone et al., 2007), or working memory and cognitive control (Aalto et al., 2005; Phillips et al., 2004; Stefani and Moghaddam, 2006), is still elusive. The fact that sustained patterns of dopamine release occur in particular target areas of dopaminergic midbrain neurons like the prefrontal cortex (Stefani and Moghaddam, 2006) suggests that functional DA diversity occurs in an anatomically ordered fashion. To study the combined anatomical, functional, and molecular properties of the mesocorticolimbic dopamine system in comparison to the mesostriatal dopamine system in adult (3-month-old) C57Bl6 mice, we carried out selective retrograde tracing experiments, combined with immunohistochemistry, electrophysiological recordings, and UV-laser-microdissection-based quantitative mRNA-expression profiling of individual DA neurons. Here, we show that the dopamine midbrain system consists indeed of two distinct types of DA midbrain neurons with nonoverlapping axonal target areas and very different molecular and functional properties. In addition to the well-studied conventional dopaminergic midbrain neurons,

we here identified an atypical fast-firing subtype of dopaminergic neurons, with very low expression of the plasma membrane dopamine transporter (DAT). Among these fast-firing DA neurons, those projecting to the prefrontal cortex were unique, as they possessed no functional somatodendritic dopamine D2 autoreceptors and expressed very low mRNA levels of D2 dopamine receptors and their downstream targets, the GIRK2 channel, at the level of individual neurons. Thus, we provide here a cellular and molecular basis for the regional and temporal diversity of dopamine signaling in the adult brain that might facilitate more selective therapeutic targeting of dopaminergic subsystems, differentially affected in disorders like schizophrenia and Parkinson disease.

## RESULTS

### Anatomical Segregation of the Different Projections of the Mesocorticolimbic Dopaminergic System in the Midbrain Suggests a Dual System

First, we mapped the anatomical distribution of retrogradely labeled and immunohistochemically identified TH-positive ($TH^+$, i.e., dopaminergic, DA) midbrain neurons for the five different mesocorticolimbic target regions: medial prefrontal cortex (mPFC), basolateral amygdala (BLA), nucleus accumbens (NAc) core, NAc medial shell, and the NAc lateral shell. For comparison, we also mapped the distribution of conventional nigrostriatal DA neurons projecting to the dorsolateral striatum (DS). Figure 1A shows the injection sites in the main target areas of the mesocorticolimbic DA system: mPFC, BLA, NAc core, and NAc medial and lateral shell. For comparison, the lowest panel shows a dorsolateral striatal injection site for labeling of the nigrostriatal DA system. While the left halves of the figures show examples of the respective injection sites, the right halves display color-coded schematic overlays of the three to five different, selective tracing experiments carried out for each of the mesocorticolimbic target areas at the same caudorostral level. Importantly, Figure S1 (available online) documents the selectivity of all injection sites used for the anatomical mapping of all six different targets by their complete caudorostral serial reconstructions. Figures 1B and 1C compare the cumulative anatomical distribution of retrogradely labeled and immunohistochemically identified TH-positive neurons for the six different target regions at the same caudorostral levels in the posterior midbrain (bregma −3.49 mm; respective areas of three distinct subnuclei of the VTA indicated by different colors). Our data show that DA neurons projecting to mPFC, BLA, and NAc core and medial shell cluster in the medial posterior VTA, where they were predominantly located both in the medial paranigral (PN) nucleus and the adjacent medioventral aspects of the parabrachial (PBP) nucleus, while only a smaller population of DA neurons with these projections were found in the adjacent interfascicular (IF) nucleus close to midline. In contrast, DA neurons projecting to the lateral shell region of the NAc were almost completely excluded from PN and were scattered throughout the PBP. Outside the VTA (A10), a significant portion of these NAc lateral shell projecting DA neurons was situated in the most medial aspects of the substantia nigra (SN, A9) pars compacta. For comparison, DA neurons projecting to the dorsolateral striatum were almost exclusively found in the SN. Complete serial reconstructions throughout the entire caudorostral span of the midbrain were carried out to define the positions of the $TH^+$ DA neurons within the VTA with the five distinct mesocorticolimbic target areas in comparison with the mesostriatal projection (see Figure S2). These data confirmed that only mPFC, BLA, and NAc core and medial shell projecting DA neurons were located within the paranigral nucleus of the VTA, where almost no DA neurons projecting to NAc lateral shell were found. As expected, mesostriatal DA neurons were largely restricted to the SN, and none of them were found in the PN. On the other hand, only mesostriatal and mesolimbic lateral shell DA neurons were found in the retrorubral field (RRF, A8), while mesocortical, mesoamygdaloid, and mesolimbic core and medial shell DA neurons were also located in the rostral and central linear nuclei (RLi, CLi). Finally, the average cell diameters differed significantly between these two anatomically segregated DA populations. DA neurons projecting to mPFC, NAc core, NAc medial shell, and BLA were significantly smaller compared to mesolimbic lateral shell and nigrostriatal DA neurons (mesocortical, 17.5 ± 0.4 μm, n = 118; mesoamygdaloid, 17.8 ± 0.7 μm, n = 48; mesolimbic core, 18.0 ± 0.5 μm, n = 59; mesolimbic medial shell, 17.2 ± 0.5 μm, n = 45; mesolimbic lateral shell, *21.5 ± 0.5 μm, n = 59; mesostriatal, *24.0 ± 0.7 μm, n = 64, $p < 0.001$). In summary, we show a clear dual anatomical and morphological segregation of the mesocorticolimbic DA system. As shown in Figure S3, we also detected an anatomical segregation between TH-positive and TH-negative (i.e., nondopaminergic) midbrain neurons projecting to the medial PFC. In contrast to mesoprefrontal DA neurons, which clustered in and around the paranigral nucleus in the medial posterior VTA, the PN was almost devoid of TH-negative mesocortical neurons, which instead were found in both more caudal and rostral territories of the midbrain.

To study the independence of the distinct components of the mesocorticolimbic DA projection system, we carried out double-tracing experiments combining tracer injections of latex beads with red fluorochromes to mPFC with green latex beads to either the core or the lateral shell region of NAc. Respective injection sites are shown in Figure 2A. Again, DA neurons were identified by positive TH immunoreactivity (blue, Figure 2B). We found mesocortical and mesolimbic core projecting DA neurons in immediate proximity (Figure 2B, left panel), while mesocortical and mesolimbic lateral shell DA neurons were significantly more segregated and never direct neighbors (Figure 2B, right panel, and Figure 2C). In addition, these double-labeling experiments also showed that the vast majority of distinct mesocorticolimbic DA projections were organized as independent parallel lines indicated by the only small percentage of single DA neurons that harbored both green and red beads (12.5%, 4 of 32 mesocortical and mesolimbic core cells; 4.3%, 1 of 23 mesocortical and mesolimbic lateral shell cells, Figure 2D).

### Quantitative mRNA Expression Profiling for the Different Projections of the Dopaminergic Midbrain System Reveals the Dual Nature of the Mesocorticolimbic Dopamine System

To address the question whether the five different parallel projections of the mesocorticolimbic DA system, anatomically

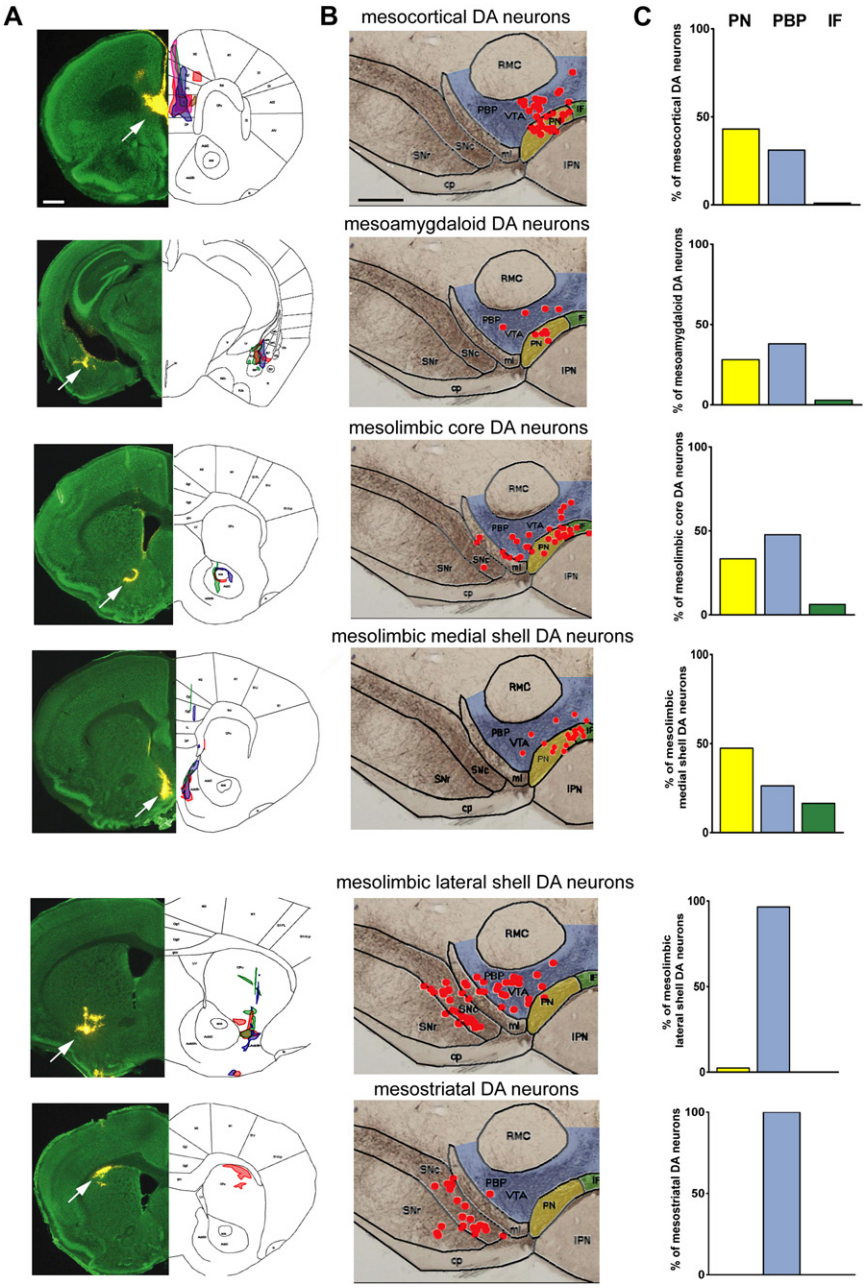


**Figure 1. Topography and Anatomical Segregation of Different Projections of the Mesocorticolimbic Midbrain System in Adult Mice**

(A) Injection sites for retrograde tracing experiments using fluorescently labeled latex beads. (Left panels) Injection sites in green nissl (488 nm) counterstained 100 μm coronal sections from top to bottom for mPFC (bregma +1.70 mm), BLA (bregma −1.94 mm), NAc core (bregma +0.98 mm), NAc medial shell (bregma +1.34 mm), NAc lateral shell (bregma +0.86 mm), DS (bregma +1.10 mm). Arrows indicate the injected reservoir of tracer beads. (Right panels) A schematic drawing of the corresponding brain regions and outline of the anatomical positions of the tracer depots. The respective tracer areas of the individual experiments in each target region (mPFC: n = 5, BLA: n = 3, NAc core: n = 3, NAc medial shell: n = 3, NAc lateral shell: n = 3, DS: n = 1) are marked with different colors. Scale bars, 500 μm.

(B) Anatomical positions of retrogradely labeled DA neurons in schematic drawings of the coronal ventral midbrain including SN and VTA regions at bregma −3.49 mm. Different subnuclei of the VTA are color coded: paranigral (PN) = yellow, parabrachial (PBP) = blue, interfascicularis (IF) = green. Red dots represent the positions of individual tracer-bead-containing and TH-immunopositive neurons in VTA and SN accumulated from one to five independent tracing experiments shown in corresponding panels in (A).

(C) Relative distribution of retrogradely labeled DA neurons between the three main VTA (A10) subnuclei PN, PBP, and IF. Note that a substantial percentage of DA VTA neurons projecting to mPFC (43.1%), BLA (28.1%), NAc core (33.4%), and NAc medial shell (47.4%) are located in PN, while mesolimbic lateral shell DA VTA neurons (2.4%) and mesostriatal DA neurons (0%) are almost or completely absent from PN.

defined as shown above, were also distinct at a molecular level, we quantified mRNA expression of important dopaminergic marker genes, tyrosine hydroxylase (TH), the vesicular monoamine transporter 2 (VMAT2), and the plasma membrane dopamine transporter (DAT), which define dopamine synthesis, packaging, and reuptake capacity of DA neurons, that project to either mPFC, BLA, NAc core, or NAc medial or lateral shell. Again for comparison, conventional nigrostriatal DA neurons projecting to the dorsolateral striatum were also studied. As shown for two of the six studied DA populations in Figures 3A–3C, after verified target-specific in vivo tracing, selective pools of five bead-labeled neurons each were collected via UV-laser microdissection (LMD) from coronal fixed cryosections for subsequent cDNA synthesis followed by quantitative real-time PCR (Liss et al., 2005). Bead-labeled DA neurons with different projections showed the same topographical distributions within the midbrain as described above (Figures 3A and 3E; compare to Figure 1). As shown in Figures 3D and 3E, the quantitative mRNA expression of TH, DAT, and VMAT2 were determined in parallel for each pool of five DA neurons with defined axonal projections. In line with our anatomical data, two significantly different patterns of TH-DAT-VMAT2 coexpression were observed (compare Figures 3D and 3E), which are shown as relative DAT/TH and DAT/VMAT2 expression ratios in Figures 3F and 3G, respectively. Mesocorticolimbic DA neurons projecting to mPFC, BLA, or NAc core or NAc medial shell displayed similarly low DAT/TH expression ratios (relative DAT/TH ratios normalized to that of mesocortical DA neurons: mesocortical 1.00 ± 0.12, n = 11;

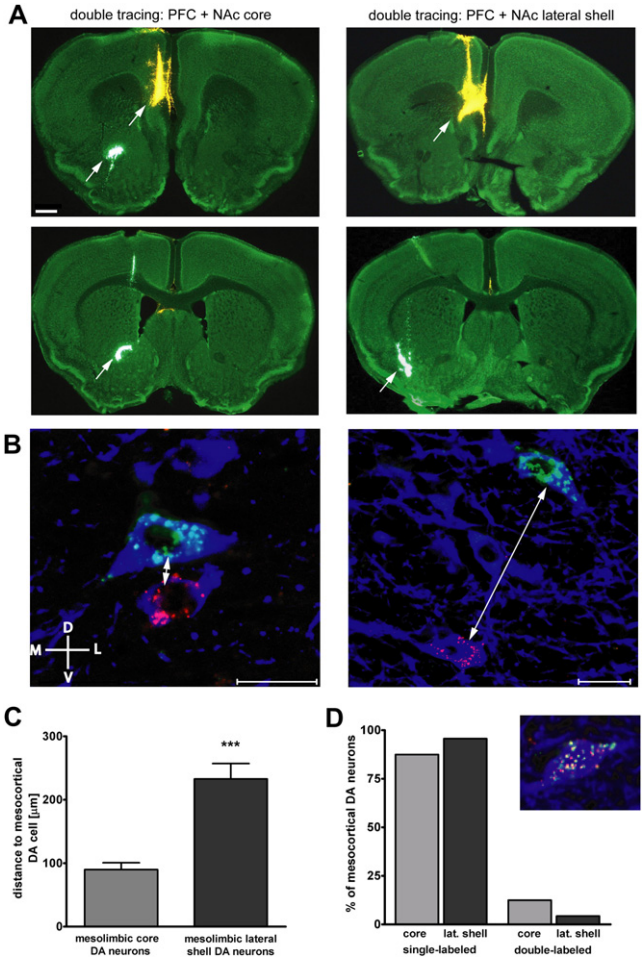


**Figure 2. Double Tracing of the Mesocorticolimbic Dopaminergic System Shows Independence and Spatial Organization of Its Distinct Projections**

(A) Injection sites (arrows) in green nissl counterstained 100 μm sections of double retrograde tracing experiments using red fluorescently labeled latex beads for mPFC and green fluorescently labeled beads for injections into NAc core (left panels) or NAc lateral shell (right panels). Sections at bregma +1.34 mm (upper panels), +0.86 mm (lower panels). Scale bar, 500 μm.

(B) Confocal images of TH-immunopositive (blue) cells in the VTA labeled with red beads for mesocortical neurons and with green beads for NAc core (left panel) or NAc lateral shell (right panel) neurons, respectively. Arrows indicate the distance between two labeled cells. Scale bars, 20 μm.

(C) Somata of mesolimbic core projecting DA neurons are significantly ($p < 0.001$) closer (83.9 ± 10.7 μm, n = 28 pairs, cumulative data from three independent experiments) to identified mesocortical DA neurons than to those of mesolimbic lateral shell DA neurons to mesocortical DA neurons (232.7 ± 24.3 μm, n = 26 pairs, cumulative data from three independent experiments). Data are presented as means ± SEM.

(D) Cortical and subcortical projections of the mesocorticolimbic DA system are largely independent parallel systems. Only 12.5% (n = 4 of 32 cells) or 4.3% (n = 1 of 23 cells) of mesocortical DA VTA neurons are double labeled after double tracing of mPFC and core or lateral shell of NAc, respectively. Insert shows an example of a double-labeled DA neuron.

mesoamygdaloid 1.32 ± 0.41; n = 12; mesolimbic core 1.87 ± 0.33, n = 15; mesolimbic medial shell 1.27 ± 0.14, n = 20). In contrast, DAT/TH expression ratios of NAc lateral shell projecting DA neurons (3.61 ± 0.50, n = 16) and of mesostriatal DA SN neurons (5.20 ± 0.22, n = 20; Figure 3F) were significantly higher. The different DAT/TH ratios resulted mainly due to large differences in DAT expression.

A similar pattern emerged when comparing the DAT/VMAT2 expression ratios. Again, mesocorticolimbic DA neurons projecting to mPFC, BLA, or NAc core or medial shell shared similar low DAT/VMAT2 expression ratios (DAT/VMAT2 ratios normalized to mesocortical DA neurons: mesocortical 1.00 ± 0.19, n = 8; mesoamygdaloid 1.24 ± 0.25, n = 10; mesolimbic core 1.51 ± 0.17, n = 13; mesolimbic medial shell 1.14 ± 0.13, n = 19) compared to the significantly higher ratios of mesolimbic lateral shell (2.95 ± 0.50, n = 15) and mesostriatal DA neurons (2.81 ± 0.38, n = 20; Figure 3G). In essence, while mesolimbic lateral shell VTA DA neurons shared the elevated DAT/TH and DAT/VMAT2 mRNA expression ratios with the mesostriatal DA SN neurons, all other constituents of the mesocorticolimbic DA system formed—in line with their anatomical segregation—a different group with significantly smaller DAT/TH as well as DAT/VMAT2 mRNA expression ratios, caused by lower DAT mRNA levels. These differences in relative DAT expression were confirmed at the protein level by multilabeling immunohistochemistry and confocal analysis. As shown in Figures 3H and 3I, somatodendritic DAT immunoreactivity of retrogradely identified mesocortical, TH-positive neurons was in most cases not significantly different from background (n = 12 of 16; 75%), compared to the strong DAT immunoreactivity in retrogradely identified mesostriatal DA SN neurons, which was found to be above background in all analyzed neurons (n = 16 of 16; 100%). DA neurons projecting to BLA (n = 12 of 14; 87%), NAc core (n = 12 of 23; 52%), and NAc medial shell (n = 11 of 20; 55%) also showed weak DAT immunoreactivity, while in contrast all analyzed mesolimbic lateral shell projecting DA neurons possessed strong DAT immunoreactivity (n = 12 of 12; 100%), similar to mesostriatal DA SN neurons. Corresponding differences in DAT immunoreactivities were also evident in the respective axonal target areas (see Figure S4). A similar analysis of calbindin d28k immunoreactivity showed that all DA neurons projecting to mPFC (n = 38 of 38 cells), to BLA (n = 9 of 9 cells), to NAc core (n = 16 of 16 cells), and to NAc medial shell (n = 8 of 8 cells) were calbindin immunopositive. However, so were also 60% of DA neurons projecting to NAc lateral shell (n = 12 of 20 cells) (see Figure S5A). Thus, in contrast to the significant differences in DAT/TH and DAT/VMAT2 expression ratios, calbindin d28k expression alone was not a fully reliable marker to differentiate between the two distinct subtypes of mesocorticolimbic DA neurons.

As shown in Figure S5B, mesocortical DA neurons not only coexpressed TH, DAT, and VMAT2, but also, like conventional nigrostriatal DA neurons, dopa decarboxylase (DDC), which renders these unconventional TH-positive neurons fully competent not only to take up and package dopamine but also to produce it enzymatically. However, their synthetic capacity for catecholamines was restricted to dopamine, as they did not coexpress TH and dopamine-β-hydroxylase (DBH) to produce norepinephrine. (in contrast to mPFC-projecting locus coeruleus neurons; compare Figures S5C and S5D).

### The Dual Mesocorticolimbic Dopamine System Is Composed of Two Distinct Functional Dopaminergic Cell Types in a Projection-Specific Manner

To address the key question whether the anatomical and molecular differences described above within the adult mesocorticolimbic DA VTA system also extend into the electrophysiological domain, we combined retrograde tracing with standard whole-cell and perforated-patch patch-clamp recordings in in vitro brain slices from 3-month-old adult C57Bl6 mice to study the basic electrophysiological properties of these two distinct neuronal dopaminergic subtypes. As in a previous study (Liss et al., 2005), we confirmed the stereotypical and well-characterized electrophysiological properties of nigrostriatal DA SN neurons (Figures 4A and 4B). Figure 4B shows a single action potential (AP) from a perforated-patch recording of a retrogradely identified mesostriatal SN DA neuron with its typical low threshold, broad AP, and prominent afterhyperpolarization (AHP). For detailed analysis of individual APs, only those perforated-patch recordings with uncompensated series resistances <40 MΩ were used. The second derivative of this action potential gives rise to the well-known waveform (middle panel) that has been utilized for cell identification in many in vivo extracellular studies of DA midbrain neurons (Grace and Bunney, 1984b; Ungless et al., 2004). The lower panel shows the phase plot of this AP. In perforated-patch recordings, DA SN neurons discharge in a slow regular pacemaker mode with typically broad action potentials (2.3 ± 0.5 Hz, n = 20, range 1.2–3.2 Hz). Upon injection of hyperpolarizing currents of increasing amplitudes, DA SN neurons develop the typical and prominent HCN-channel-mediated sag component in the subthreshold range (sag at −80 mV: 14.3 ± 1.0 mV, n = 4), which has routinely been used for functional identification of dopaminergic midbrain neurons. In contrast, retrogradely identified mesocortical DA VTA neurons possess highly distinct properties (Figures 4C and 4D). In perforated-patch recordings, their spontaneous discharge frequencies were in most cases faster (5.6 ± 0.7 Hz, n = 20, range 1–12 Hz, $p < 0.01$) than those of conventional mesostriatal DA neurons. Furthermore, upon injection of hyperpolarizing currents of increasing amplitudes, mesocortical DA neurons demonstrated no obvious sag components (sag at −80 mV: 2.9 ± 0.9 mV, n = 6), which corresponded to a lack of functional HCN currents in voltage-clamp recordings (data not shown). With increasing membrane hyperpolarizations, this DA subpopulation showed instead a prominent rebound inhibition with a slow return to the firing threshold (rebound delay: mesocortical 2.9 ± 0.7 s, n = 6; mesostriatal 0.5 ± 0.1 s, n = 4; $p < 0.01$). As shown in Figure 4D, the durations of the APs in perforated-patch recordings were even longer than those of conventional DA SN neurons (AP duration at threshold: mesocortical 7.6 ± 1.4 ms, n = 7; mesostriatal 3.5 ± 0.3 ms, n = 9; $p < 0.01$). Prominently, they also lacked a clear afterhyperpolarization (AHP: mesocortical −49.8 ± 3.1 mV, n = 9; mesostriatal −60.7 ± 1.2 mV, n = 14; $p < 0.01$). Their phase plot also indicated significantly smaller maximal depolarization (mesocortical: 24.4 ± 2.9 $mVms^{-1}$, n = 5; mesostriatal: 86.5 ± 8.3 $mVms^{-1}$, n = 5; $p < 0.01$) and repolarization speeds compared to those of mesostriatal DA neurons (mesocortical: −14.9 ± 4.9 $mVms^{-1}$, n = 5; mesostriatal: −51.6 ± 3.0 $mVms^{-1}$, n = 5; $p < 0.01$). Consequently, the second derivative of the AP waveform generated only a very small, biphasic signal, which might be more difficult to detect in vivo by extracellular recordings compared to that of mesostriatal DA neurons.

To address the question whether these very different, "unconventional" functional phenotypes of mesocorticolimbic DA neurons were associated in a systematic fashion with the distinct anatomical and molecular subgroups defined above, we combined retrograde tracing with standard whole-cell recordings, neurobiotin filling, and immunohistochemistry, which allowed electrophysiological analysis of retrogradely identified neurons and unequivocal determination of the dopaminergic phenotype for the same cell. In standard whole-cell recordings, uncompensated series resistances were routinely <25 MΩ and allowed analysis of fully resolved action potentials (e.g., mesocortical DA neurons 15.1 ± 2.2 MΩ, n = 10). The data shown in Figures 5A–5C compare the AP discharge of retrogradely identified $TH^+$ neurons (Figure 5A) with defined axonal projections in response to 2 s ramps of depolarizing currents at different amplitudes to study the dynamic firing ranges of the respective DA subtypes. In response to small current levels (Figure 5B, ramp max +50 pA), DA neurons projecting to mPFC, BLA, NAc core, and NAc medial shell discharged in a frequency range of 10–15 Hz (mPFC: 14.3 ± 1.1, n = 6; BLA: 11.8 ± 0.7, n = 9; NA core: 11.8 ± 1.1, n = 8; NAc medial shell: 11.5 ± 1.4, n = 8), while those DA neurons projecting to NAc lateral shell or to dorsolateral striatum fired action potentials in a significantly lower, 3–6 Hz frequency band (NAc lateral shell: 5.7 ± 0.5, n = 10; DS: 4.8 ± 0.2, n = 5, $p < 0.001$). In response to increasingly higher ramp currents, all DA subtypes showed depolarization block after reaching their maximal firing frequencies (Figure 5C). Again, the DA neurons projecting to mPFC, BLA, NAc core, and NAc medial shell showed significantly higher maximal discharge frequencies in the range of 20–30 Hz (mPFC: 24.8 ± 2.9, n = 13; BLA: 19.5 ± 1.1, n = 9; NAc core: 21.1 ± 2.3, n = 8; NAc medial shell: 22.9 ± 2.7, n = 8), well above those DA neurons that projected to NAc lateral shell and DS (NAc lateral shell: 9.0 ± 0.4, n = 28; DS: 9.5 ± 0.6, n = 13, $p < 0.001$, Figure 5D). The latter remained in a frequency band below 10 Hz, consistent with the well-described maximal tonic firing ranges of conventional DA neurons in vivo and in vitro (Grace and Bunney, 1984b; Liss et al., 2005). Moreover, the fast-firing DA phenotypes were able to sustain higher firing ranges above the conventional upper limit of 10 Hz for at least several seconds during ramp depolarizations, in contrast to the conventional DA neurons (Figure 5E) that might only reach higher firing-frequencies during subsecond burst discharges in vitro and in vivo (Grace and Bunney, 1984a; Wolfart and Roeper, 2002). Thus, adding to their anatomical segregation and their quantitative molecular differences, the two DA phenotypes identified here are able to operate within two distinct frequency bands and temporal domains. A variety of additional electrophysiological data for the six retrogradely identified DA subgroups (depicted in Figure S6) further confirmed the clear functional distinctions between unconventional VTA DA neurons projecting to mPFC, BLA, NAc core, and medial shell compared to those projecting to NAc lateral shell that possessed—like mesostriatal DA SN neurons—the well-described classical DA phenotype. DA neurons projecting

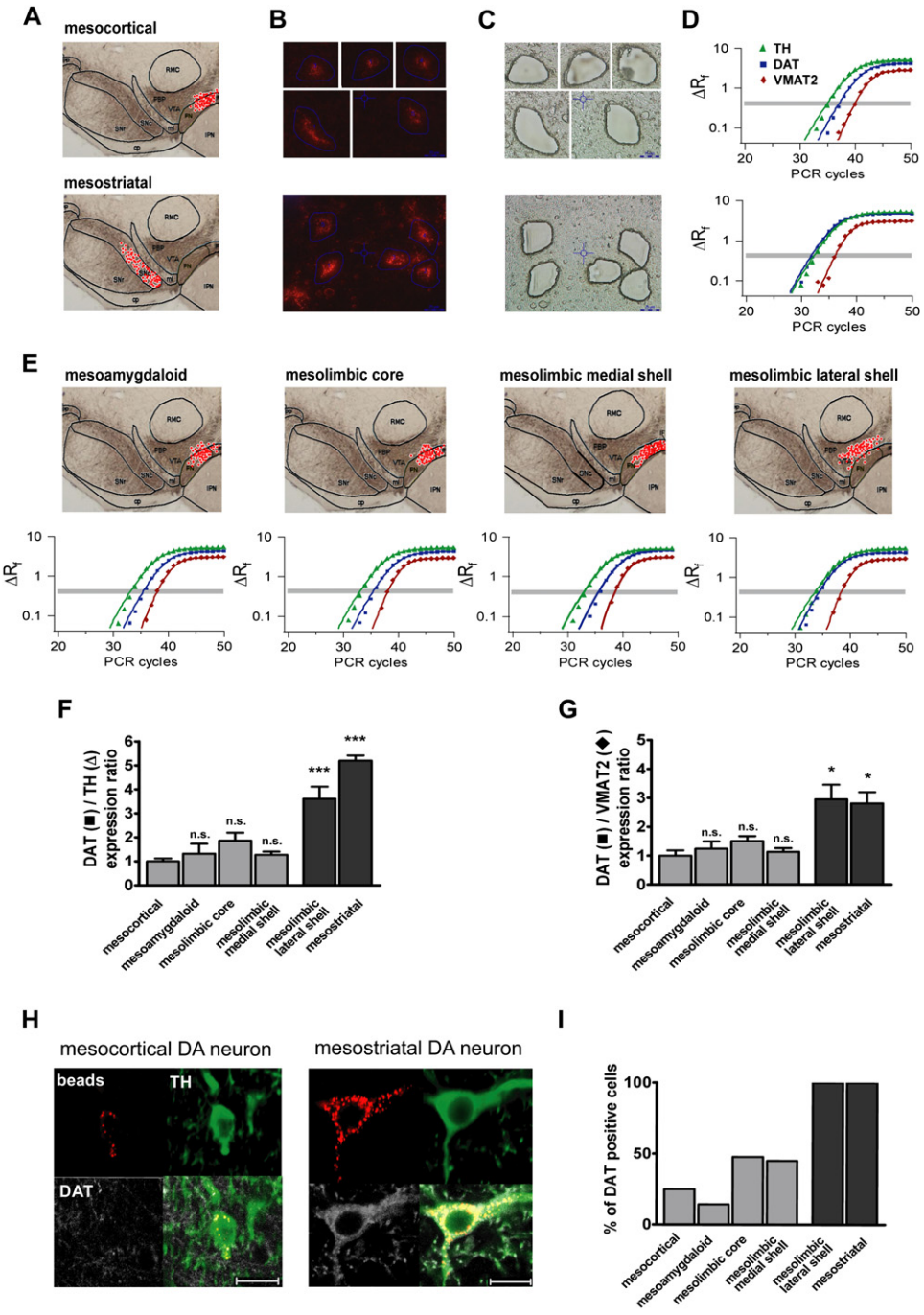


**Figure 3. Quantitative RT-PCR of Retrogradely Labeled, Laser-Microdissected Neurons Indicates Two Molecularly Distinct Neuronal Subtypes in the Mesocorticolimbic Dopamine System**

(A and E) (Upper row) Anatomical positions of retrogradely labeled, UV-LMD collected DA neurons (as in Figure 1B), accumulated from one to four independent tracing experiments (PFC: n = 3, BLA: n = 4, NAc core: n = 2, NAc medial shell: n = 2, NAc lateral shell: n = 2, DS: n = 2).

(B and C) Fluorescence (B) and bright-field DIC (C) images (LMD6000) of five bead-containing individual DA neurons with different projection sites, manually marked under fluorescence illumination before (B) and after (C) UV-LMD. Scale bars, 25 μm.

(D and E) (Lower row) Semilogarithmic real-time PCR amplification plots for DAT (blue square), TH (green triangle), and VMAT2 (red diamond) using cDNA from labeled cell pools (compare [B] and [C]) as templates. Grey lines indicate Ct-line of analysis. Note the earlier detection (= lower Ct value) of DAT in cells projecting to the DS and NAc lateral shell compared to those projecting to NAc core, NAc medial shell, BLA, or PFC.

to mPFC, BLA, and NAc core and medial shell also possessed similar AP waveforms (Figure S6A) that were significantly longer (mPFC: 6.7 ± 0.6 ms, n = 15; BLA: 6.5 ± 0.7 ms, n = 9; NAc core: 4.4 ± 0.2 ms, n = 7; NAc medial shell: 4.5 ± 0.4 ms, n = 6; Figure S6B) and had much smaller AHPs (mPFC: −47.7 ± 1.6 mV, n = 15, BLA: −39.0 ± 1.8 mV, n = 9; NAc core: −41.2 ± 1.2 mV, n = 7; NAc medial shell: −41.7 ± 2.1 mV, n = 6; Figure S6C) compared to DA neurons projecting to NAc lateral shell and DS (AP duration at threshold: NAc lateral shell 3.2 ± 0.1 ms, n = 12; DS 3.1 ± 0.2 ms, n = 13; AHP: NAc lateral shell −56.9 ± 1.8 mV, n = 12; DS −57.4 ± 1.2 mV, n = 10). In addition, all unconventional DA neurons of the mesocorticolimbic system showed little to no sag components followed by long rebound inhibitions in response to hyperpolarizing currents (sag −80 mV: mPFC 3.8 ± 0.5 mV, n = 12; BLA 3.4 ± 0.6 mV, n = 9; NAc core 6.2 ± 1.5 mV, n = 13; NAc medial shell 4.1 ± 1.0 mV, n = 8; rebound delay: mPFC 2.2 ± 0.5 s, n = 12; BLA 3.0 ± 0.5 s, n = 7; NAc core 2.8 ± 0.5 s, n = 13; NAc medial shell 2.5 ± 0.5 s, n = 8). This subthreshold behavior was very different compared to conventional mesolimbic lateral shell and mesostriatal DA neurons (sag −80 mV: NAc lateral shell 14.4 ± 1.0, n = 36; DS 19.0 ± 0.8, n = 15; rebound delay: NAc lateral shell 0.9 ± 0.2, n = 16; DS 0.4 ± 0.1, n = 11, Figures S6A, S6D, and S6E).

In order to test the emerging dual nature of the dopaminergic midbrain system and the existence of a second type of mesocorticolimbic DA midbrain neuron in an unbiased manner, we carried out an unsupervised hierarchical cluster analysis based on a set of seven electrophysiological properties for 44 individual DA midbrain neurons (pF, AP threshold [mV], AP duration [ms], AHP [mV], max. firing rate [Hz], min. and max. speed of voltage change during AP [mV/ms]). As shown in Figure S7, this analysis indeed revealed two highly distinct (Wilk's $\lambda = 0.170$, $p < 0.001$) groups of DA neurons, which for almost all cells (n = 41 of 44) were in accordance with two distinct groups of DA neurons based on their differences in axonal projections and gene expression described above. A discrimination analysis revealed that the AHP amplitude was the single most reliable functional property to functionally discriminate the two distinct types of DA neurons. The more subtle separation into several subgroups within the two robust DA clusters showed smaller differences between mesolimbic lateral shell and mesostriatal DA neurons, as previously described (Liss et al., 2005), but linked no subgroups exclusively to their respective axonal projection area. These clustering data independently confirmed the existence of two highly distinct subtypes of dopaminergic midbrain neurons, with nonoverlapping axonal targets and associated systematic differences in gene expression.

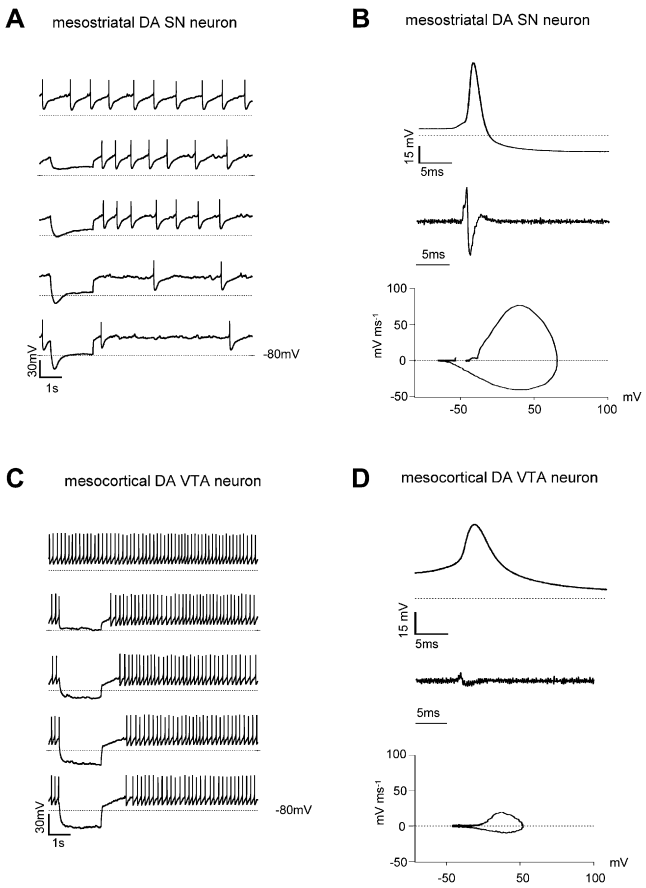


**Figure 4. The Dopaminergic Midbrain System Is Composed of Two Highly Distinct Functional Phenotypes**

(A) Gramicidin-perforated-patch recordings of an identified mesostriatal DA neuron from 3-month-old mouse in current-clamp mode. Note slow regular discharge with pronounced afterhyperpolarizations (AHPs) and sag components induced by injections of hyperpolarizing currents of increasing amplitudes (steps of −25 pA).

(B) Gramicidin-perforated-patch recordings of an identified mesostriatal DA neuron from 3-month-old mouse in current-clamp mode. Note typical action potential (AP) waveform (upper panel). Second derivative of the AP is shown in middle panel. Lower panel shows the phase plot ($mVms^{-1}$/mV) of the AP.

(C) Gramicidin-perforated-patch recordings of an identified mesocortical DA neuron from 3-month-old mouse in current-clamp mode. Note fast regular discharge and absence of AHPs and sag components. Injections of hyperpolarizing currents as in (A).

(D) Gramicidin-perforated-patch recordings of an identified mesocortical DA neuron from 3-month-old mouse in current-clamp mode. Note broad AP waveform without AHP (upper panel). Second derivative of the AP is shown in middle panel. Note the small amplitude in comparison to (B). Lower panel shows the phase plot ($mVms^{-1}$/mV) of the AP with smaller maximal depolarization and repolarization speeds.

(F and G) Statistical analysis of real-time PCR experiments. DA neurons projecting to NAc core, NAc medial shell, BLA, and PFC show significantly lower DAT/TH expression ratios as well as lower DAT/VMAT2 expression ratios relative to neurons projecting to NAc lateral shell or DS (ratios normalized; PFC = 1). Data are presented as means ± SEM.

(H) Confocal images of DAT immunoreactivity (white) of TH-immunopositive (green) cells labeled with red beads for mesocortical DA neurons (left panel) or mesostriatal DA neurons (right panel). Scale bar, 20 μm.

(I) Only 25% (n = 4 of 16 cells) of mesocortical DA neurons, 14% (n = 2 of 14 cells) of mesoamygdaloid DA neurons, 48% (n = 11 of 23 cells) of mesolimbic core DA, and 45% (n = 9 of 20 cells) of mesolimbic medial shell DA neurons showed DAT immunoreactivity above background. In contrast, DAT immunoreactivity was significantly different from background in all analyzed mesolimbic lateral shell (n = 12 of 12 cells) and mesostriatal DA neurons (n = 16 of 16 cells).

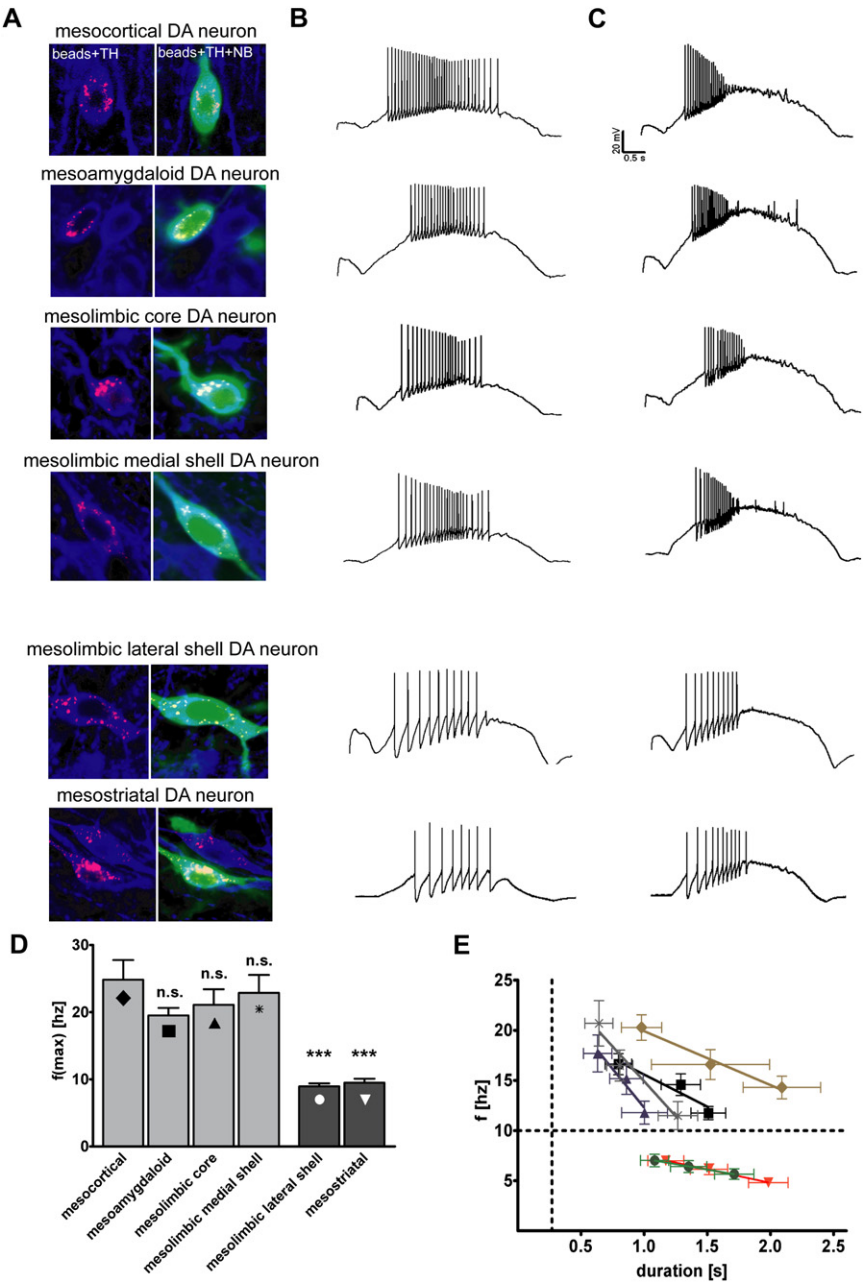


**Figure 5. The Two Anatomically Segregated Functional Phenotypes of the Dopaminergic Midbrain System Operate in Different Frequency Bands**

(A) Confocal analysis of individual retrogradely labeled (red beads), recorded, neurobiotin-filled (green), and TH-immunopositive (blue) neurons.

(B and C) Whole-cell, current-clamp responses to 2 s ramps of small depolarizing currents (+50 pA) of the retrogradely identified DA neurons. Note that mesocortical, mesoamygdaloid, mesolimbic core, and mesolimbic medial shell DA neurons discharge even in response to small current injections in a higher frequency range compared to mesolimbic lateral shell and mesostriatal DA neurons. (C) During 2 s ramp current injections of larger amplitudes (100–200 pA), all DA subtypes showed depolarization block of spontaneous electrical activity after discharging at different maximal frequencies (scale bars: 20 mV, 500 ms). Note reduction of AP amplitudes in fast-firing DA neurons before onset of depolarization block.

(D) Mean maximal firing rates of retrogradely identified DA neurons induced by ramp depolarizations. Mesocortical (24.8 ± 2.9 Hz, n = 13), mesoamygdaloid (19.5 ± 1.1 Hz, n = 9), mesolimbic core (21.1 ± 2.3 Hz, n = 8), and mesolimbic medial shell (22.9 ± 2.7 Hz, n = 8) DA neurons showed significantly higher maximal discharge rates compared to mesolimbic lateral shell (9.0 ± 0.4 Hz, n = 28) and mesostriatal (9.5 ± 0.6 Hz, n = 13) DA neurons ($p < 0.001$). Data are presented as means ± SEM.

(E) Mesocortical (brown, n = 6), mesoamygdaloid (black, n = 9), mesolimbic core (blue, n = 8), and mesolimbic medial shell (gray, n = 8) DA neurons are able to sustain higher firing ranges above the conventional upper limit of 10 Hz (dashed horizontal line) for several seconds during 2 s ramp depolarization of small depolarizing currents (+50 pA, +100 pA, + 150 pA). In contrast, mesolimbic lateral shell (green, n = 10) and mesostriatal (red, n = 5) DA neurons could only maintain rates below this limit for several seconds. (The dashed vertical line at 270 ms indicates the average duration of phasic high-frequency bursting in conventional midbrain DA neurons.) Data are presented as means ± SEM.

## Mesoprefrontal Dopamine Neurons Are Unique within the Dual DA Midbrain System Due to Their Lack of Functional Somatodendritic D2 Autoreceptors

Another criterion—with important therapeutic implications—that has been widely used to define DA midbrain neurons is the inhibition of their electrical activity by stimulation of somatodendritic D2-type dopamine autoreceptors, which in turn activate G protein-coupled potassium channels (e.g., GIRK2, Kir3.2) and thereby hyperpolarize the plasma membrane (Beckstead et al., 2004). We carried out perforated-patch-clamp recordings to monitor effects of dopamine on spontaneous electrical activity of retrogradely identified DA neurons from all six anatomically defined groups. For maximal stimulation of both synaptic and extrasynaptic D2 autoreceptors on the somatodendritic membrane (Beckstead and Williams, 2007), we bath applied 100 μM dopamine, which led to membrane hyperpolarization (−61.7 ± 4.7 mV, n = 7) accompanied by a complete and stable cessation of spontaneous electrical activity (7 of 7 cells, Figure 6C) in all tested mesostriatal DA SN neurons. Very similar to mesostriatal DA neurons, electrical activity was completely suppressed throughout the dopamine bath application in all mesolimbic DA VTA neurons projecting to the lateral shell region of the NAc (−63.8 ± 1.0 mV, n = 7, Figure 6B) and only slowly returned after the washout of dopamine. Similar, pacemaker activities of mesoamygdaloid DA VTA neurons (−59.1 ± 3.5 mV, n = 3, Figure 6C), mesolimbic core DA neurons (−62.8 ± 7.3 mV, n = 5, Figure 6C),

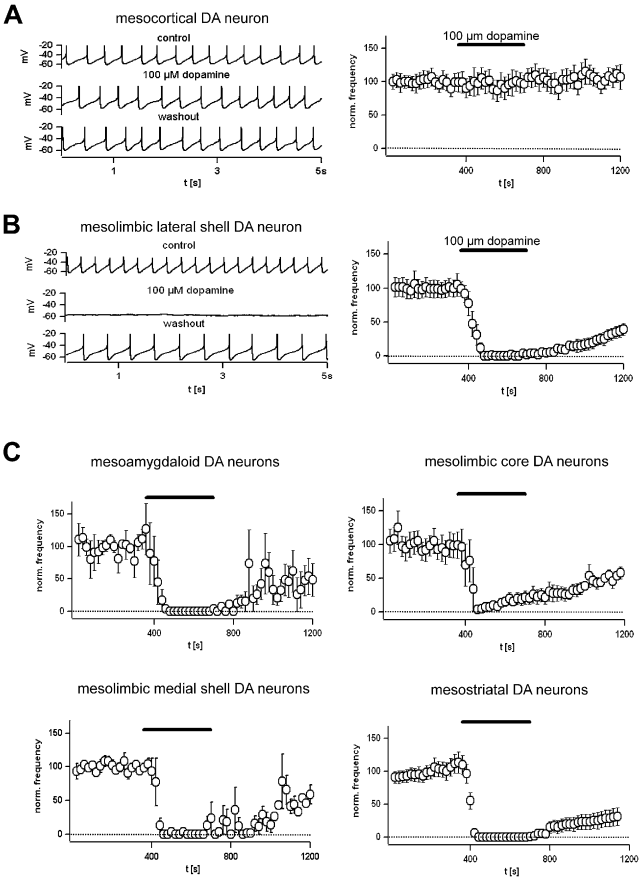


**Figure 6. Mesoprefrontal Dopamine Neurons Are Unique Due to Their Absence of Functional Somatodendritic D2 Autoreceptors**

(A and B) Gramicidin-perforated-patch recordings of identified mesocortical DA neuron (A) and mesolimbic lateral shell DA neuron (B). Left panels show electrical activity in control (upper), in the presence of 100 µM dopamine (middle), and after washout of dopamine (lower). Right panels plot the normalized mean spontaneous discharge frequencies before, during, and after dopamine application for identified mesocortical DA neurons (n = 7) and mesolimbic lateral shell DA neurons (n = 7). Note the complete absence of dopamine-mediated inhibition in mesocortical DA neurons and the complete and sustained inhibition of mesolimbic lateral shell DA neurons by dopamine. Data are presented as means ± SEM.

(C) Normalized mean spontaneous discharge frequencies of identified mesoamygdaloid DA neurons (n = 3), mesolimbic core (n = 5), mesolimbic medial shell (n = 3), and mesostriatal (n = 7) DA neurons before, during, and after application of 100 µM dopamine. Note that complete inhibition of electrical activity was not fully sustained in mesoamygdaloid, mesolimbic core, and mesolimbic medial shell DA subtypes. Data are presented as means ± SEM.

and mesolimbic medial shell DA neurons (−69.0 ± 4.5 mV, n = 3, Figure 6C) were also completely suppressed by 100 µM dopamine. However, in contrast to all other DA VTA neurons of the mesocorticolimbic system, only those projecting to mPFC did not respond to dopamine application in all tested cells (n = 7, Figure 6A). These differences in D2 autoreceptor signaling demonstrate that mesocortical DA neurons possess unique properties within the framework of a dual DA midbrain system. The absence of D2 receptor-mediated inhibition of mesocortical DA neurons was selective for dopamine and not due to a general failure of inhibition by neurotransmitter application. As shown in Figure S8, similar to nigrostriatal DA neurons, mesocortical DA neurons were readily hyperpolarized and electrically silenced by bath application of either 1 mM GABA (mesocortical: −62.7 ± 4.7, n = 3; nigrostriatal: −76.8 ± 2.5 mV, n = 4) or 10 µM baclofen (mesocortical: −66.2 ± 8.5, n = 3; nigrostriatal: −84.1 ± 1.2 mV, n = 4).

## Low Expression Levels of D2 Dopamine Receptor and GIRK2 Channel mRNAs in Single Mesocortical DA Neurons

To study the molecular nature of this observed difference in somatodendritic D2 autoreceptor responses between mesocortical DA neurons and all other DA midbrain populations, we again turned to cell-specific UV-laser microdissection of retrogradely identified DA neurons. Via RT-qPCR, we quantified mRNA of D2 receptors and GIRK2 channels in single neurons with defined axonal projections. To minimize the effects of interindividual differences, we carried out double tracings of mesocortical and mesostriatal DA neurons. Figure 7A shows examples of differently labeled mesocortical and mesostriatal DA neurons within the same animal before UV-laser microdissection of individual traced neurons, while Figure 7B plots relative positions of all analyzed neurons within the ventral midbrain (compare Figure 1). The single-cell cDNA of each individual DA neuron was purified and split for quantitative PCR of D2 and GIRK2. Figures 7C–7E show that individual mesostriatal DA neurons possessed at least one order of magnitude higher mRNA levels of both GIRK2 and D2 compared to those of mesocortical DA neurons (GIRK2, 10.0-fold: 3.84 ± 0.93, n = 11 of 20 mesocortical; 38.48 ± 0.24, n = 25 of 30 mesostriatal. D2, 14.7-fold: 2.60 ± 0.80, n = 8 of 20 mesocortical; 38.28 ± 0.27, n = 26 of 30 mesostriatal). As we analyzed the expression of GIRK2 and D2 in parallel in single mesocortical or mesostriatal DA neurons, we could also determine the single-cell expression ratios of these two genes for individual neurons. While GIRK2 and D2 mRNA were codetected in most (80%, n = 24 of 30) of the tested single mesostriatal DA neurons, only in 25% (n = 5 of 20) of mesocortical DA neurons were both transcripts detected. In contrast to the significant differences in mRNA abundances for both GIRK2 and D2 between the two different types of dopaminergic neurons, their respective expression ratios were very similar (mesostriatal: 0.84 ± 0.11, n = 24; mesocortical: 0.76 ± 0.31, n = 5, Figure 7G), indicating that these genes were tightly coregulated across different DA subtypes.

We finally wished to study also the differences of GIRK2 and D2 protein expression between these two types of dopaminergic neurons. Unfortunately, none of the four different D2 antibodies tested showed specific immunostaining when compared to corresponding sections of a D2 knockout mouse (see Experimental Procedures)—forcing us to restrict our analysis to GIRK2 immunoreactivity. As shown in Figure 8, we carried out a semiquantitative analysis of GIRK2 immunoreactivities for retrogradely identified mesocortical and mesostriatal DA subpopulations (see Experimental Procedures and Supplemental Data for details). While the GIRK2 immunosignals of mesocortical DA neurons were close to background (cell/background ratio mPFC: 1.5 ± 0.1, n = 10), consistent with the low mRNA

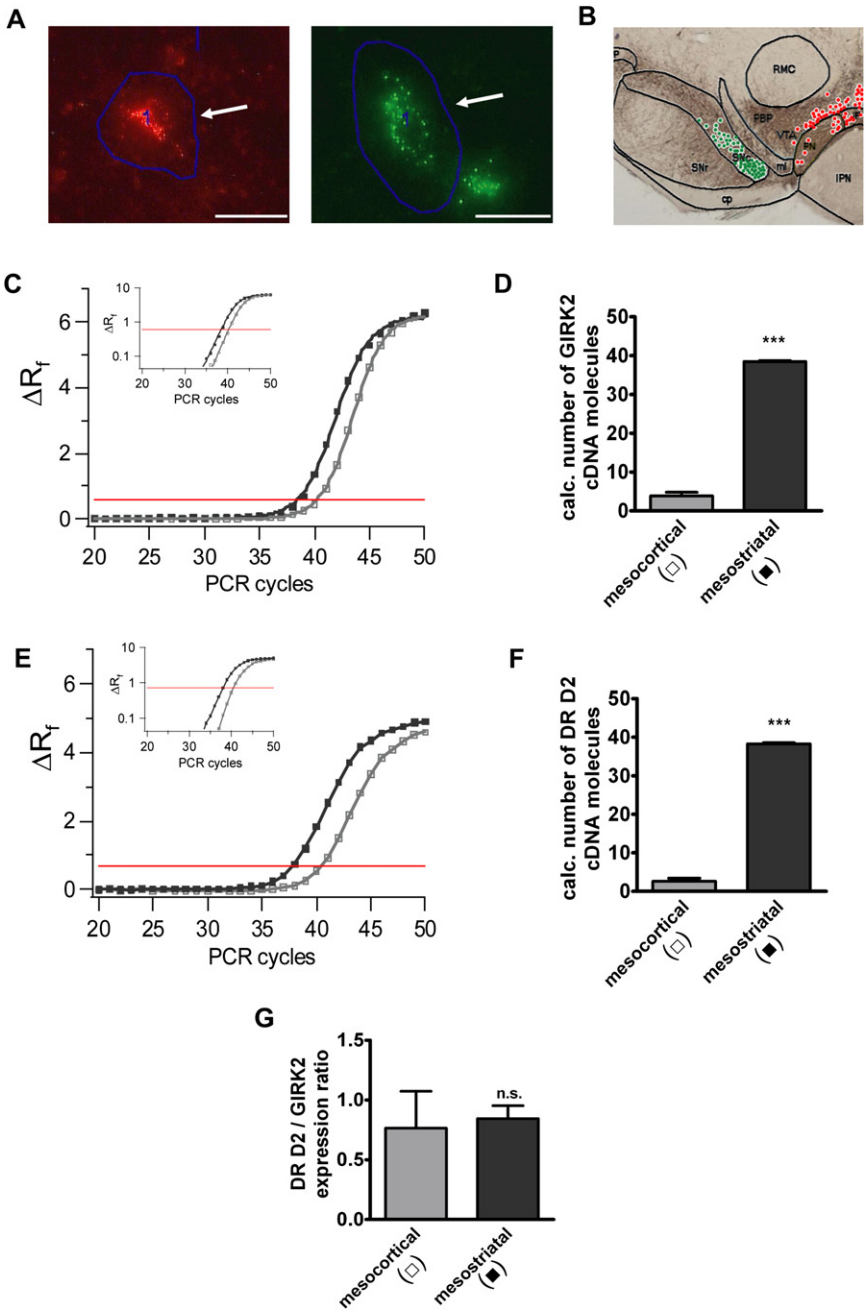


**Figure 7. Quantitative Single-Cell RT-PCR Reveals Lower Abundance of GIRK2 and D2 mRNA in Mesocortical Compared to Mesostriatal Dopaminergic Neurons**

(A) LMD6000 images of bead-containing individual DA neurons (indicated by arrow), projecting to mPFC (left, red beads) or DS (right, green beads) of a double-traced animal before UV-laser microdissection. Scale bars, 25 μm.

(B) Relative anatomical positions of retrogradely labeled individual mesocortical (red dots) and mesostriatal (green dots) DA neurons collected via UV-LMD (three independent tracing experiments).

(C and E) Real-time PCR amplification plots of GIRK2 (upper) and D2 (lower) of individual retrogradely identified neurons, one projecting to mPFC (gray squares), the other to dorsolateral striatum (black squares). Inserts show semilogarithmic amplification plots. Red lines indicate Ct-lines for analysis. Note the detection (Ct-value) of GIRK2 and D2 at lower PCR cycles in the mesostriatal compared to the mesocortical DA neuron.

(D and F) Calculated number of GIRK2 (upper) and D2 (lower) mRNA molecules are significantly lower in mesocortical DA neurons (gray bars: GIRK2: 3.84 ± 0.93, n = 11 of 20; D2: 2.60 ± 0.80, n = 8 of 20) compared to mesostriatal DA neurons (black bars: GIRK2: 38.48 ± 0.24, n = 25 of 30; D2: 38.28 ± 0.27, n = 26 of 30). Data are presented as means ± SEM.

(G) Single-cell D2/GIRK2 mRNA expression ratios of mesocortical (0.76 ± 0.31, n = 5 of 20) and mesostriatal (0.84 ± 0.11, n = 24 of 30) DA neurons are not significantly different. Data are presented as means ± SEM.

abundance of GIRK2 and the absent D2/GIRK2-mediated inhibition of these DA neurons, the GIRK2 immunosignals of mesostriatal DA SN neurons were almost 5-fold larger compared to background (DS: 4.6 ± 0.5, n = 10, Figure 8C).

## DISCUSSION

Our study demonstrates that the adult dopaminergic midbrain system is composed of two different, functionally and molecularly distinct types of dopaminergic neurons with anatomical segregation in the midbrain and nonoverlapping axonal targets. Among this dual system, DA neurons projecting to medial prefrontal cortex are unique due to their absence of functional somatodendritic D2 receptors. Our findings help to resolve a debate about the degree of cellular diversity within the dopaminergic midbrain system (Chiodo et al., 1984; Deniau et al., 1980; Gariano et al., 1989; Shepard and German, 1984). Chiodo and colleagues (Chiodo et al., 1984) presented evidence that DA neurons projecting to cortical areas possessed distinct in vivo properties compared to "conventional" nigrostriatal DA neurons, which either discharged in a pacemaker mode below 10 Hz or in short bursts at higher frequencies (Grace et al., 2007). These functional differences included higher pacemaker frequencies and the apparent lack of inhibition by somatodendritic D2 autoreceptors, another hallmark of conventional DA midbrain neurons (Beckstead et al., 2004). However, other groups did not find evidence for these fast-firing, atypical mesocortical DA neurons (Deniau et al., 1980; Gariano et al., 1989; Shepard and German, 1984). More recent in vitro brain slice studies of DA midbrain neurons (Ford et al., 2006; Liss et al., 2005; Margolis et al., 2006a) accumulated further evidence that DA midbrain neurons differed in certain electrophysiological

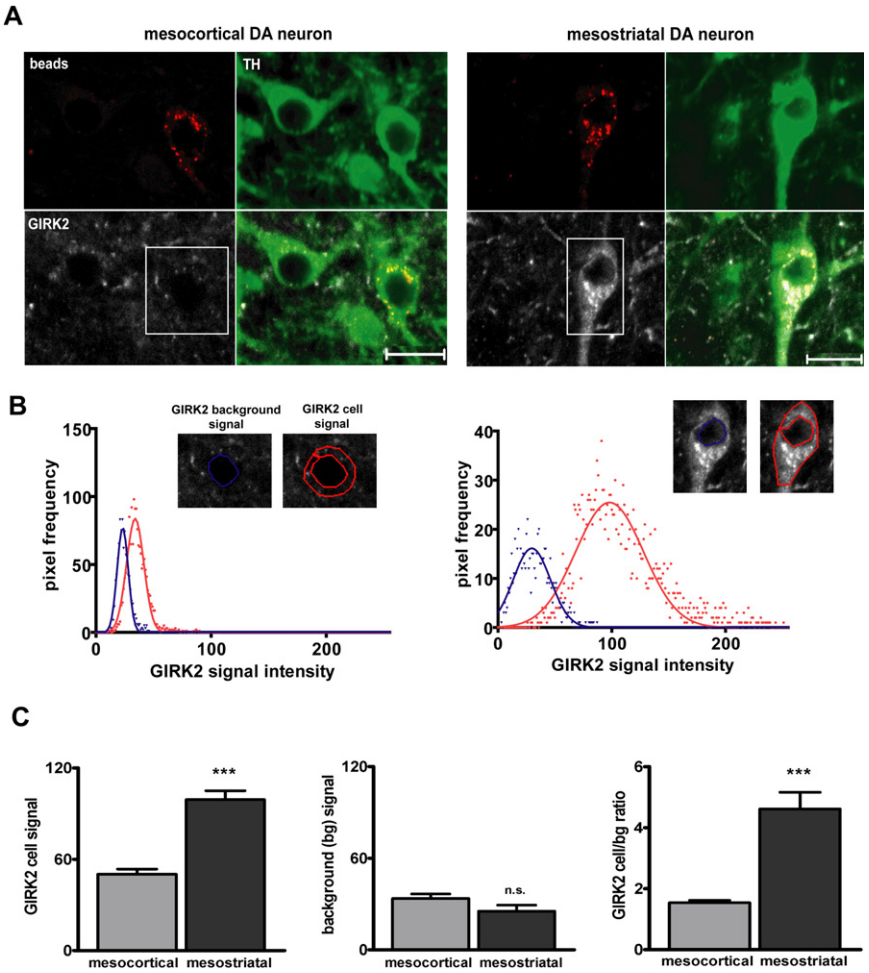


**Figure 8. Differences in GIRK2 Immunoreactivities between Mesocortical and Mesostriatal DA Neurons**

(A) Confocal images of GIRK2 immunoreactivity (white) of TH-immunopositive (green) cells labeled with red beads for mesocortical DA neurons (left panel) or mesostriatal DA neurons (right panel). Overlays are shown in lower right panels. Scale bars, 20 μm.

(B) Frequency distributions of nuclear GIRK2 background signal (blue) and the cellular GIRK2 signal (red) for the mesocortical and mesostriatal DA neurons shown in (A). Insets indicate region of interests (ROI) for GIRK2 cellular and nuclear background signal.

(C) Mean cellular GIRK2 immunosignals for retrogradely identified mesocortical (50.2 ± 3.3, n = 10) and mesostriatal DA neurons (mesostriatal: 99.2 ± 5.9, n = 10, $p < 0.001$, left panel). GIRK2 background signals were not significantly different (mesocortical: 33.6 ± 3.0, n = 10; mesostriatal: 25.3 ± 3.9, n = 10, $p > 0.05$, middle panel). Significantly higher GIRK2 cell/background ratios for mesostriatal (4.6 ± 0.5, n = 10, $p < 0.001$) compared to mesocortical DA neurons (1.5 ± 0.1, n = 10, right panel). Data are presented as means ± SEM.

and modulatory properties (Margolis et al., 2006b; Neuhoff et al., 2002; Wolfart et al., 2001). However, a general scheme combining the levels of recognized anatomical, functional, and molecular diversity of the adult DA midbrain system did not emerge (Bjorklund and Dunnett, 2007a, 2007b). Such a scheme is essential to define the cellular basis for the temporal and regional variety of behaviorally relevant dopamine signaling in the brain (Schultz, 2007).

We show here that mesocorticolimbic DA midbrain neurons projecting selectively to medial prefrontal cortex, basolateral amygdala, and the core and the medial shell of nucleus accumbens are able to fire action potentials at significantly higher frequencies in a sustained fashion compared to the "conventional" DA neurons (<10 Hz). Among these fast-firing DA neurons, only mesocortical DA neurons were not inhibited by somatodendritic D2 receptor activation. The ability of these DA subtypes to fire at higher frequencies in a sustained fashion is a candidate mechanism that could contribute to the more sustained DA release pattern in vivo recognized in particular in the amygdala and the prefrontal cortex (Garris and Wightman, 1994; Mundorf et al., 2001). In the case of the mesocortical DA neurons, the lack of somatodendritic dopamine inhibition would further facilitate sustained electrical discharge and release. The linear increase in prefrontal dopamine overflow in vivo in response to medial forebrain bundle stimulations in a range between 20 and 60 Hz (Yavich et al., 2007) supports our notion that sustained fast firing of mesocorticolimbic DA neurons could shape the temporal pattern of dopamine in its axonal target areas.

Once dopamine is released, DAT-mediated reuptake is one of the key mechanisms that defines decay kinetics of extracellular dopamine concentrations. We show here that mesocortical DA neurons possess the lowest DAT mRNA expression compared to all other DA subtypes. Also, DAT/TH and DAT/VMAT2 mRNA expression ratios were lowest in mesocortical DA neurons. Thus, a small dopamine reuptake capacity relative to TH-mediated synthesis and VMAT2-mediated vesicular packaging of dopamine is expected to contribute to the 10-fold slower decay of extracellular dopamine concentrations in cortical areas compared to those in dorsal striatum (Yavich et al., 2007). Thus, based on the combination of our functional and molecular data, the fast-firing mesocorticolimbic DA neurons with a low dopamine reuptake capacity appear well suited to mediate the often sustained forms of behaviorally relevant DA release in vivo in several brain regions (Bassareo et al., 2002; Floresco et al., 2003; Schultz, 2007; Stefani and Moghaddam, 2006) (notwithstanding the ongoing technical debate of temporal resolution and specificity of DA detection in vivo [Wightman, 2006]). Given these considerations, atypical DA midbrain neurons might be specifically involved in, for example, working memory (Phillips et al., 2004; Seamans and Yang, 2004; Stefani and Moghaddam, 2006), fear conditioning (Marowsky et al., 2005; Rosenkranz and Grace, 2002), or drug addiction (Cardinal et al., 2001; Dalley

et al., 2007; Everitt and Robbins, 2005). However, the fact that DA neurons projecting to either prefrontal cortex or medial shell of the nucleus accumbens, which share the fast-firing electrophysiological phenotype and possess very similar DAT/TH and DAT/VMAT2 expression ratios, are known to give rise to very different patterns of DA release in vivo might serve as a reminder that additional factors, such as size and density of the axonal terminal regions, presynaptic regulation, and plasticity, etc., also shape the temporal profile of extracellular dopamine (Schmitz et al., 2003). In addition, insights into differences in synaptic connectivity (Carr et al., 1999; Carr and Sesack, 2000) and plasticity (Martin et al., 2006; Ungless et al., 2003) between DA subtypes are equally important for our understanding of their various behavioral roles in vivo. Future studies using in vivo recordings of these unconventional DA neurons will be critical to further define their distinct functional roles and the relation between their electrical activity and dopamine release.

The uniquely absent D2 autoreceptor-mediated inhibition of electrical activity of mesocortical DA neurons could play an important role in the context of the well-known differential effects of antipsychotics. This might be further exploited for more selective targeting of the dopaminergic subsystems. This study provides a set of available molecular markers (DAT, TH, VMAT2, D2, GIRK2—but not calbindin d28k) that will reliably allow the identification and discrimination of the dopaminergic subtypes. In contrast, we found no clear evidence for a coexpression of dopaminergic with glutamatergic marker genes in the mesocorticolimbic system, which has been discussed as a potentially differential marker by previous studies (Lavin et al., 2005), but rather an anatomical segregation of ascending dopaminergic and nondopaminergic midbrain systems. Although our analysis of the DA midbrain system was restricted to the adult mouse brain, where anatomical, functional, and molecular approaches can be combined, our findings will also facilitate the analysis of diversity in the largely expanded DA midbrain system of primates and humans (Haber, 2003), where distinct DA subtypes regarding DAT and D2 abundance have already been described (Haber et al., 1995; Lewis et al., 2001). The established combination of single-cell UV-laser microdissection and quantitative mRNA expression profiling for human DA midbrain neurons from post mortem brains (Ramirez et al., 2006) will allow probing of the human DA midbrain system. In analogy to our findings in mouse brain, mesocortical DA neurons might be identified by their low D2 and GIRK2 expression levels combined with their low DAT/TH and DAT/VMAT2 mRNA ratios and in addition by their expected low mRNA abundances for SK3 (Wolfart et al., 2001) and HCN channel subunits (Neuhoff et al., 2002).

Taken together, the anatomical, molecular, and functional identification of a subtype of mesocorticolimbic dopaminergic midbrain neuron, and its specific projections to medial prefrontal cortex, basolateral amygdala, and nucleus accumbens core and medial shell, offer rational cellular and molecular targets for more selective therapeutic interventions into the dopaminergic midbrain system, in particular, for specific pharmacological modulation of electrical activity and dopamine release of the mesocorticolimbic DA system, for example, in diseases like schizophrenia (Winterer and Weinberger, 2004), drug abuse (Everitt and Robbins, 2005), and ADHD (Arnsten, 2006), where either altered cortical or limbic dopamine signaling are key features of the pathophysiology. The desired subtype-specific pharmacological modulation (either stimulation or inhibition) of the distinct dopaminergic midbrain projections also holds the long-term promise of reducing the high prevalence of severe side effects in current treatments of major diseases like schizophrenia (Fleischhacker and Widschwendter, 2006) and Parkinson's disease (Weintraub and Stern, 2005).

## EXPERIMENTAL PROCEDURES

### Retrograde Tracing

Essentially as already described (Liss et al., 2005). In all experiments, male adult (3-month-old) C57Bl6 mice were used, and all procedures were approved by the German Regierungspräsidium Giessen and Darmstadt. For a detailed description, see Supplemental Data. Briefly, under general ketamine-dormitor anesthesia and stereotactic control (Cartesian Instruments), retrobeads (Lumafluor, Naples, F) were injected unilaterally in dorsolateral striatum (DS) (bregma: 0.98 mm, lateral: 1.9 mm, ventral: 2.2 mm; 80 nl beads), nucleus accumbens (NAc) lateral shell (bregma: 1.45 mm, lateral: 1.75 mm, ventral: 4.0 mm; 80 nl beads), NAc medial shell (bregma: 1.78 mm, lateral: 0.4 mm, ventral: 4.1 mm; 80 nl beads), NAc core (bregma: 1.54 mm, lateral: 1.0 mm, ventral: 4.0 mm; 80 nl beads), basolateral amygdala (BLA) (bregma: −1.54 mm, lateral: 2.8 mm, ventral: 4.3 mm; 100 nl beads), or medial prefrontal cortex (mPFC) (quadruple injection of each 100 nl beads at four different sites: bregma: 1.95 mm, 2.05 mm, 2.15 mm, and 2.25 mm, lateral: 0.27 mm, ventral: 2.1 mm + 1.6 mm). We noticed that these empirically derived stereotaxic coordinates did not match those given in the mouse brain atlas by Franklin and Paxinos (2001), which we used as reference for our serial reconstructions (on average the caudal-rostral axis appeared to be ca. 400 μm shifted caudally). For sufficient labeling, survival periods for retrograde tracer transport depended on respective injection areas: DS and NAc lateral shell, 7 days; NAc core, NAc medial shell, and BLA, 14 days; and mPFC, 21 days.

### Electrophysiological Recordings from Adult Mouse Brain Slices

Essentially as previously described (Liss et al., 2005; Neuhoff et al., 2002). For detailed description, see Supplemental Data.

### Immunohistochemistry and Semiquantitative Analysis of GIRK2 Immunostaining

Immunohistochemistry and confocal microscopy were as previously described (Neuhoff et al., 2002; Wolfart et al., 2001). For a detailed description, see Supplemental Data.

### Brain Mapping

TH-stained coronal midbrain sections (50 μm) were reconstructed with Neurolucida Software (MicroBrightfield, Colchester, VT) by using a LUDL motor-driven microscope stage (LUDL Electronic Products, Hawthorne, NY) and the Lucivid camera system (MicroBrightfield). TH-positive and labeled cells were mapped and counted by scanning the midbrain sections with a 63×/1.25 oil lens. Sections were located relative to Bregma by using landmarks and neuroanatomical nomenclature as described in the Franklin and Paxinos mouse brain atlas (Franklin and Paxinos, 2001).

### UV-Laser Microdissection

Laser microdissection (LMD) was performed essentially as already described (Liss et al., 2005), using an LMD6000 system (Leica Microsystems). Coronal cryosections (12 μm) of mouse midbrains were cut (Leica cryostat CM1850), mounted on RNase-free UV-light-treated membrane slides (1 mm polyethylene-naphthalate membrane, MicroDissect), fixed with ethanol (75% [−20°C], 75%, 95%, 100%, 100% [RT each]), and air dried. Retrobead-labeled neurons were visualized (63× objective) and marked under fluorescence illumination (red beads: N2.1 filter, 515–560 nm excitation; green beads: L5 filter, 480 ± 40 nm excitation). Fluorescence-labeled neurons were cut under bright-field

DIC microscopy and collected by gravity directly into a cap of a 0.5 ml thin-walled PCR-tube (Applied Biosystems). The mixture for cell lysis and cDNA synthesis was added directly into the lid, and reverse transcription was performed as described (Liss et al., 2005; Ramirez et al., 2006).

### Quantitative Real-Time PCR (TaqMan Primer/Probes)

Purification of cDNA and quantitative real-time PCR were essentially as previously described (Liss et al., 2001, 2005). cDNA pellet was dissolved in appropriate volumes of molecular biology grade water (5 μl per assay) for 1–2 hr at 45°C. One-half of purified single-cell cDNA (for simultaneous D2 and GIRK2 quantification), or one-third of cell-pool cDNA (for simultaneous TH, DAT, and VMAT2 detection) each was used as templates in 20 μl PCR reactions with QuantiTect Probe PCR Master Mix (QIAGEN, no UNG, ROX as passive reference dye). Real-time TaqMan assays were either obtained from Applied Biosystems (D2, GIRK2) or from Metabion (TH, DAT, VMAT2). For a more detailed description, see Supplemental Data.

### Statistics

Student's t tests or one-way ANOVA tests were used to determine statistical differences using GraphPad prism 5 (Graphpad Software, San Diego, CA). Bonferroni post hoc analysis was applied, when necessary, to compare means. Statistical significance was set at $p < 0.05$. All data values are presented as means ± SEM.

## SUPPLEMENTAL DATA

The Supplemental Data for this article can be found online at http://www.neuron.org/cgi/content/full/57/5/760/DC1/.

## ACKNOWLEDGMENTS

We thank Guido Schemken and his staff for excellent animal care; E. Naudascher, B. Jordan, S. Petzoldt, and A-L. Damm for excellent technical support. We thank Dr. E. Borrelli for providing D2 KO mouse brains, Dr. A.I. Levey for D2 polyclonal antibodies, and Leica Microsystems for the LMD6000. We are grateful for the MRC support (I.J. and J.R.) during pilot experiments at the MRC Neuroanatomical Pharmacology Unit, Oxford (data not shown). The study was supported by Gemeinnützige Hertie Stiftung, Nationales Genomforschungs Netzwerk (NGFNII, BmbF), Förderfonds Goethe University Frankfurt and Interdisciplinary Center for Neuroscience (ICN), Frankfurt. B.L. is supported by the Alfried Krupp prize for young university teachers of the Krupp foundation. Retrograde tracing, immunohistochemistry, and anatomical reconstruction were by S.L., I.J., and J.R. Laser microdissection and molecular biology were by A.H., O.H., and B.L. Electrophysiology was by S.L. and J.R. The study was designed and the manuscript written by B.L. and J.R. B.L. is a consultant for Leica Microsystems.

Received: August 10, 2007
Revised: December 17, 2007
Accepted: January 11, 2008
Published: March 12, 2008

## REFERENCES

Aalto, S., Bruck, A., Laine, M., Nagren, K., and Rinne, J.O. (2005). Frontal and temporal dopamine release during working memory and attention tasks in healthy humans: a positron emission tomography study using the high-affinity dopamine D2 receptor ligand [11C]FLB 457. J. Neurosci. *25*, 2471–2477.

Arnsten, A.F. (2006). Stimulants: Therapeutic actions in ADHD. Neuropsychopharmacology *31*, 2376–2383.

Bassareo, V., De Luca, M.A., and Di Chiara, G. (2002). Differential expression of motivational stimulus properties by dopamine in nucleus accumbens shell versus core and prefrontal cortex. J. Neurosci. *22*, 4709–4719.

Beckstead, M.J., and Williams, J.T. (2007). Long-term depression of a dopamine IPSC. J. Neurosci. *27*, 2074–2080.

Beckstead, M.J., Grandy, D.K., Wickman, K., and Williams, J.T. (2004). Vesicular dopamine release elicits an inhibitory postsynaptic current in midbrain dopamine neurons. Neuron *42*, 939–946.

Berridge, K.C. (2007). The debate over dopamine's role in reward: the case for incentive salience. Psychopharmacology (Berl.) *191*, 391–431.

Bjorklund, A., and Dunnett, S.B. (2007a). Dopamine neuron systems in the brain: an update. Trends Neurosci. *30*, 194–202.

Bjorklund, A., and Dunnett, S.B. (2007b). Fifty years of dopamine research. Trends Neurosci. *30*, 185–187.

Cardinal, R.N., Pennicott, D.R., Sugathapala, C.L., Robbins, T.W., and Everitt, B.J. (2001). Impulsive choice induced in rats by lesions of the nucleus accumbens core. Science *292*, 2499–2501.

Carr, D.B., and Sesack, S.R. (2000). Projections from the rat prefrontal cortex to the ventral tegmental area: target specificity in the synaptic associations with mesoaccumbens and mesocortical neurons. J. Neurosci. *20*, 3864–3873.

Carr, D.B., O'Donnell, P., Card, J.P., and Sesack, S.R. (1999). Dopamine terminals in the rat prefrontal cortex synapse on pyramidal cells that project to the nucleus accumbens. J. Neurosci. *19*, 11049–11060.

Chiodo, L.A., Bannon, M.J., Grace, A.A., Roth, R.H., and Bunney, B.S. (1984). Evidence for the absence of impulse-regulating somatodendritic and synthesis-modulating nerve terminal autoreceptors on subpopulations of mesocortical dopamine neurons. Neuroscience *12*, 1–16.

Dalley, J.W., Fryer, T.D., Brichard, L., Robinson, E.S., Theobald, D.E., Laane, K., Pena, Y., Murphy, E.R., Shah, Y., Probst, K., et al. (2007). Nucleus accumbens D2/3 receptors predict trait impulsivity and cocaine reinforcement. Science *315*, 1267–1270.

Deniau, J.M., Thierry, A.M., and Feger, J. (1980). Electrophysiological identification of mesencephalic ventromedial tegmental (VMT) neurons projecting to the frontal cortex, septum and nucleus accumbens. Brain Res. *189*, 315–326.

Di Chiara, G., and Bassareo, V. (2007). Reward system and addiction: what dopamine does and doesn't do. Curr. Opin. Pharmacol. *7*, 69–76.

Everitt, B.J., and Robbins, T.W. (2005). Neural systems of reinforcement for drug addiction: from actions to habits to compulsion. Nat. Neurosci. *8*, 1481–1489.

Fiorillo, C.D., Tobler, P.N., and Schultz, W. (2003). Discrete coding of reward probability and uncertainty by dopamine neurons. Science *299*, 1898–1902.

Fleischhacker, W.W., and Widschwendter, C.G. (2006). Treatment of schizophrenia patients: comparing new-generation antipsychotics to each other. Curr. Opin. Psychiatry *19*, 128–134.

Floresco, S.B., West, A.R., Ash, B., Moore, H., and Grace, A.A. (2003). Afferent modulation of dopamine neuron firing differentially regulates tonic and phasic dopamine transmission. Nat. Neurosci. *6*, 968–973.

Ford, C.P., Mark, G.P., and Williams, J.T. (2006). Properties and opioid inhibition of mesolimbic dopamine neurons vary according to target location. J. Neurosci. *26*, 2788–2797.

Franklin, G., and Paxinos, K.B.J. (2001). The Mouse Brain in Stereotaxic Coordinates (San Francisco, CA: Academic Press).

Gariano, R.F., Tepper, J.M., Sawyer, S.F., Young, S.J., and Groves, P.M. (1989). Mesocortical dopaminergic neurons. 1. Electrophysiological properties and evidence for soma-dendritic autoreceptors. Brain Res. Bull. *22*, 511–516.

Garris, P.A., and Wightman, R.M. (1994). Different kinetics govern dopaminergic transmission in the amygdala, prefrontal cortex, and striatum: an in vivo voltammetric study. J. Neurosci. *14*, 442–450.

Grace, A.A., and Bunney, B.S. (1984a). The control of firing pattern in nigral dopamine neurons: burst firing. J. Neurosci. *4*, 2877–2890.

Grace, A.A., and Bunney, B.S. (1984b). The control of firing pattern in nigral dopamine neurons: single spike firing. J. Neurosci. *4*, 2866–2876.

Grace, A.A., Floresco, S.B., Goto, Y., and Lodge, D.J. (2007). Regulation of firing of dopaminergic neurons and control of goal-directed behaviors. Trends Neurosci. *30*, 220–227.

Haber, S.N. (2003). The primate basal ganglia: parallel and integrative networks. J. Chem. Neuroanat. *26*, 317–330.

Haber, S.N., Ryoo, H., Cox, C., and Lu, W. (1995). Subsets of midbrain dopaminergic neurons in monkeys are distinguished by different levels of mRNA for the dopamine transporter: comparison with the mRNA for the D2 receptor, tyrosine hydroxylase and calbindin immunoreactivity. J. Comp. Neurol. *362*, 400–410.

Lavin, A., Nogueira, L., Lapish, C.C., Wightman, R.M., Phillips, P.E., and Seamans, J.K. (2005). Mesocortical dopamine neurons operate in distinct temporal domains using multimodal signaling. J. Neurosci. *25*, 5013–5023.

Lewis, D.A., Melchitzky, D.S., Sesack, S.R., Whitehead, R.E., Auh, S., and Sampson, A. (2001). Dopamine transporter immunoreactivity in monkey cerebral cortex: regional, laminar, and ultrastructural localization. J. Comp. Neurol. *432*, 119–136.

Liss, B., Franz, O., Sewing, S., Bruns, R., Neuhoff, H., and Roeper, J. (2001). Tuning pacemaker frequency of individual dopaminergic neurons by Kv4.3L and KChip3.1 transcription. EMBO J. *20*, 5715–5724.

Liss, B., Haeckel, O., Wildmann, J., Miki, T., Seino, S., and Roeper, J. (2005). K-ATP channels promote the differential degeneration of dopaminergic midbrain neurons. Nat. Neurosci. *8*, 1742–1751.

Margolis, E.B., Lock, H., Chefer, V.I., Shippenberg, T.S., Hjelmstad, G.O., and Fields, H.L. (2006a). Kappa opioids selectively control dopaminergic neurons projecting to the prefrontal cortex. Proc. Natl. Acad. Sci. USA *103*, 2938–2942.

Margolis, E.B., Lock, H., Hjelmstad, G.O., and Fields, H.L. (2006b). The ventral tegmental area revisited: is there an electrophysiological marker for dopaminergic neurons? J. Physiol. *577*, 907–924.

Marowsky, A., Yanagawa, Y., Obata, K., and Vogt, K.E. (2005). A specialized subclass of interneurons mediates dopaminergic facilitation of amygdala function. Neuron *48*, 1025–1037.

Martin, M., Chen, B.T., Hopf, F.W., Bowers, M.S., and Bonci, A. (2006). Cocaine self-administration selectively abolishes LTD in the core of the nucleus accumbens. Nat. Neurosci. *9*, 868–869.

Mundorf, M.L., Joseph, J.D., Austin, C.M., Caron, M.G., and Wightman, R.M. (2001). Catecholamine release and uptake in the mouse prefrontal cortex. J. Neurochem. *79*, 130–142.

Neuhoff, H., Neu, A., Liss, B., and Roeper, J. (2002). I(h) channels contribute to the different functional properties of identified dopaminergic subpopulations in the midbrain. J. Neurosci. *22*, 1290–1302.

Phillips, A.G., Ahn, S., and Floresco, S.B. (2004). Magnitude of dopamine release in medial prefrontal cortex predicts accuracy of memory on a delayed response task. J. Neurosci. *24*, 547–553.

Ramirez, A., Heimbach, A., Grundemann, J., Stiller, B., Hampshire, D., Cid, L.P., Goebel, I., Mubaidin, A.F., Wriekat, A.L., Roeper, J., et al. (2006). Hereditary parkinsonism with dementia is caused by mutations in ATP13A2, encoding a lysosomal type 5 P-type ATPase. Nat. Genet. *38*, 1184–1191.

Rosenkranz, J.A., and Grace, A.A. (2002). Dopamine-mediated modulation of odour-evoked amygdala potentials during pavlovian conditioning. Nature *417*, 282–287.

Salamone, J.D., Correa, M., Farrar, A., and Mingote, S.M. (2007). Effort-related functions of nucleus accumbens dopamine and associated forebrain circuits. Psychopharmacology (Berl) *191*, 461–482.

Schmitz, Y., Benoit-Marand, M., Gonon, F., and Sulzer, D. (2003). Presynaptic regulation of dopaminergic neurotransmission. J. Neurochem. *87*, 273–289.

Schultz, W. (2007). Behavioral dopamine signals. Trends Neurosci. *30*, 203–210.

Seamans, J.K., and Yang, C.R. (2004). The principal features and mechanisms of dopamine modulation in the prefrontal cortex. Prog. Neurobiol. *74*, 1–58.

Shepard, P.D., and German, D.C. (1984). A subpopulation of mesocortical dopamine neurons possesses autoreceptors. Eur. J. Pharmacol. *98*, 455–456.

Stefani, M.R., and Moghaddam, B. (2006). Rule learning and reward contingency are associated with dissociable patterns of dopamine activation in the rat prefrontal cortex, nucleus accumbens, and dorsal striatum. J. Neurosci. *26*, 8810–8818.

Tobler, P.N., Fiorillo, C.D., and Schultz, W. (2005). Adaptive coding of reward value by dopamine neurons. Science *307*, 1642–1645.

Ungless, M.A., Singh, V., Crowder, T.L., Yaka, R., Ron, D., and Bonci, A. (2003). Corticotropin-releasing factor requires CRF binding protein to potentiate NMDA receptors via CRF receptor 2 in dopamine neurons. Neuron *39*, 401–407.

Ungless, M.A., Magill, P.J., and Bolam, J.P. (2004). Uniform inhibition of dopamine neurons in the ventral tegmental area by aversive stimuli. Science *303*, 2040–2042.

Weintraub, D., and Stern, M.B. (2005). Psychiatric complications in Parkinson disease. Am. J. Geriatr. Psychiatry *13*, 844–851.

Wightman, R.M. (2006). Detection technologies. Probing cellular chemistry in biological systems with microelectrodes. Science *311*, 1570–1574.

Winterer, G., and Weinberger, D.R. (2004). Genes, dopamine and cortical signal-to-noise ratio in schizophrenia. Trends Neurosci. *27*, 683–690.

Wolfart, J., and Roeper, J. (2002). Selective coupling of T-type calcium channels to SK potassium channels prevents intrinsic bursting in dopaminergic midbrain neurons. J. Neurosci. *22*, 3404–3413.

Wolfart, J., Neuhoff, H., Franz, O., and Roeper, J. (2001). Differential expression of the small-conductance, calcium-activated potassium channel SK3 is critical for pacemaker control in dopaminergic midbrain neurons. J. Neurosci. *21*, 3443–3456.

Yavich, L., Forsberg, M.M., Karayiorgou, M., Gogos, J.A., and Mannisto, P.T. (2007). Site-specific role of catechol-O-methyltransferase in dopamine overflow within prefrontal cortex and dorsal striatum. J. Neurosci. *27*, 10196–10209.